Dynamical correlations in one-dimensional charge-transfer insulators

Karlo Penc[1,2] and Walter Stephan[1,3]
[1]*Max-Planck-Institut für Physik komplexer Systeme, Nöthnitzer Strasse 38, D-01187 Dresden, Germany*
[2]*Research Institute for Solid State Physics and Optics, H-1525 Budapest, P.O.B. 49, Hungary*
[3]*Department of Physics, Bishop's University, Lennoxville, Québec, Canada J1M 1Z7*
(Received 26 July 2000)

The single-particle spectral function and the density response of a two band Emery model for CuO chains is calculated for large on-site Cu repulsion U and large on-site energy difference Δ. For $U \gg U-\Delta \gg t$ the eigenfunctions are products of charge and spin parts, which allows analytical calculation of spectral functions in that limit. For other parameters numerical diagonalization is used. The low-energy hole carriers are shown to be the one-dimensional analogs of the Zhang-Rice singlets. The validity of the one-band model is discussed. The results are relevant to the interpretation of photoemission and electron-energy-loss spectroscopy experiments on $SrCuO_2$ and Sr_2CuO_3.

I. INTRODUCTION

One of the most intriguing phenomena in one-dimensional electron systems is the so called spin-charge separation: the low-energy excitations are decoupled collective modes of charge and spin character, which may have different velocities, and are referred to as holons and spinons, respectively. As a consequence, the spin and charge of an added electron will be spatially separated after some time and there are no Fermi-liquid-like quasiparticles. While the decoupling exists also in the weak-coupling limit,[1] it is perhaps best understood for the strong-coupling limit of the Hubbard model, where the Bethe ansatz solution tells us that the wave functions are factorized into a part describing free spinless fermions representing the charges and a part representing the spins.[2] This allowed the calculation of the dynamical spectral functions of the Hubbard model at[3] and away[4] from half filling with excellent resolution. These calculations provided an explanation of the origin of the different features in the spectral function.

The most direct test of the theory is to look at the photoemission spectra of highly anisotropic materials. The nearly ideally one-dimensional CuO chains[5] in the charge-transfer insulators $SrCuO_2$ and Sr_2CuO_3 are perfect candidates, given that the typical energy scale for spin and charge excitations is large compared to the experimental resolution, making the observation of the low-energy spectrum possible. The absence of bands would indicate that we are not dealing with the usual quasiparticles of Fermi-liquid theory. On the other hand, there are very clear theoretical predictions for the photoemission spectrum of a system where spin-charge separation exists, and indeed, recent photoemission experiments on $SrCuO_2$ (Refs. 6–8) and photoemission[9,10] and electron-energy-loss[11] experiments on Sr_2CuO_3 seem to indicate that the dynamics at low energies can be understood within an effective t-J or Hubbard model.

In comparing the measured spectra with the theoretical ones, we face the following difficulties: (i) the actual material is a charge-transfer insulator, while the Hubbard/t-J model is a Mott insulator. Therefore one is led to question how much of the spectra can be attributed to generic features where the details of the model are not important; (ii) for the CuO_2 plane, the t-J model is derived to describe the dynamics of complex objects—the Zhang-Rice singlets.[12] In the CuO_3 chains the O ions are not all identical, and the original picture of Zhang and Rice has to be refined; (iii) on the theoretical side, apart from numerical calculations of the dynamical correlations which are difficult to interpret, exact and/or analytical results are very rare concerning the spectral function[3,13–15] and the optical conductivity (e.g., for the Hubbard model, see Ref. 16).

To answer these questions, we will consider the one-dimensional (1D) model involving the Cu ions and the oxygens between them (see Fig. 1), the so called two band Emery model,[17,18] as the simplest extension of the Hubbard model. In this paper we show that the charge-spin factorized wave function is an exact eigenfunction of the Emery model in the strong-coupling limit, however, the spinless fermions (''charges'') represent complex objects which are the one-dimensional analogs of the Zhang-Rice singlets. Furthermore, we demonstrate that the Emery model can naturally explain the reduction of spectral weight for small momenta seen experimentally[6–10] and also describes some higher energy features of the photoemission spectra.

Since the formation of Zhang-Rice singlets is an essentially strong-coupling phenomenon, the approach we present in the paper is the most suitable method to apply. Weak-coupling approaches[13] are inappropriate to capture the additional physics due to the presence of additional bands.

The outline of the paper is as follows: In Sec. II we introduce the Emery model and the canonical transformation leading to the strong-coupling effective model. The spectral

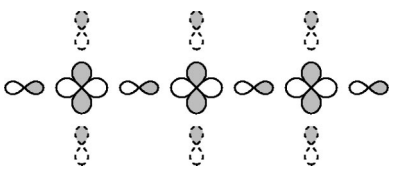

FIG. 1. The CuO_3 chain with $3d$ orbitals of Cu and $2p$ orbitals of O. The side oxygens (dashed lines) are omitted in the two band model.

functions within this effective model are calculated in Sec. III, while in Sec. IV the density-density correlations relevant to the electron-energy-loss spectroscopy (EELS) experiments are discussed.

II. EMERY MODEL

A. Definition of the model

The Emery model is given by the Hamiltonian $\mathcal{H}=\mathcal{T}+\mathcal{U}+\mathcal{V}$. For the kinetic part we take the usual tight-binding form,

$$\mathcal{T}=-t\sum_{i,\delta,\sigma}(d^{\dagger}_{i,\sigma}p_{i+\delta,\sigma}+\text{H.c.}), \tag{1}$$

where $d^{\dagger}_{i,\sigma}$ and $p^{\dagger}_{i+\delta,\sigma}$ denote the hole creation operators on copper d and oxygen p orbitals at sites i and $i+\delta$, respectively. The Cu-Cu distance is taken to be unity, i are integers and $\delta=\pm 1/2$. The phase factors in the hybridization coming from the symmetry of the Cu and O orbitals are absorbed in the definition of the d and p operators as $d_j=(-1)^j d_{\text{phys},j}$, and $p_{j+1/2}=(-1)^j p_{\text{phys},j+1/2}$, where the subscript ''phys'' denotes the operators respecting the phase factors in the hybridization. The inclusion of the phase factors causes a shift of π in the momentum of the O hole and will be explicitly mentioned when necessary. In the potential part we include the on-site energy difference $\Delta=\varepsilon_p-\varepsilon_d$ and the on-site Coulomb repulsion U of the Cu $3d$ orbitals:

$$\mathcal{U}=\frac{\Delta}{2}\sum_i (n^p_{i+1/2}-n^d_i)+U\sum_i n^d_{i,\uparrow}n^d_{i,\downarrow}, \tag{2}$$

where $n^a_{i,\sigma}=a^{\dagger}_{i,\sigma}a_{i,\sigma}$ $(a=d,p)$, and $n^a_i=\Sigma_\sigma n^a_{i,\sigma}$, furthermore, the nearest-neighbor Cu-O repulsion

$$\mathcal{V}=V\sum_{i,\delta} n^d_i n^p_{i+\delta}, \tag{3}$$

which may lead to exciton formation.[18] We choose $U>\Delta$ in order to have a charge-transfer insulator with one hole per unit cell.[19]

Note that if one begins with a model which also includes oxygen orbitals on the side of the chain, as a preliminary step one may build bonding, and anti- and nonbonding combinations of these. Therefore, if one understands our single oxygen orbital per cell to correspond to the bonding combination, our results may also be seen to represent a good approximation to part of the spectrum of the more complete four band model.[20,21]

B. Effective model in the strong-coupling limit

As mentioned earlier, direct numerical methods, such as exact diagonalization, work only for rather small system sizes. However, in the strong-coupling limit $(U,\Delta\gg t,V)$ it is possible to do controlled calculations both analytically and numerically. As a first step, we derive an effective strong-coupling Hamiltonian. In the extreme case when $t=V=0$, the Hamiltonian is block-diagonal in the subspace of states with a given eigenvalue of $\mathcal{U}$. The hybridization in $\mathcal{T}$ may be treated perturbatively using a canonical transformation,[22] leading to an effective Hamiltonian $\mathcal{H}_{\text{eff}}$ acting within one subspace. A detailed and systematic explanation for the case of the Hubbard model is given in Ref. 23. We denote by tilde (e.g., $\tilde{p}$) the operators acting in the subspace of $\mathcal{H}_{\text{eff}}$, and the physical operators $\mathcal{O}$ are then obtained from

$$\mathcal{O}=e^{\mathcal{S}}\tilde{\mathcal{O}}e^{-\mathcal{S}}=\tilde{\mathcal{O}}+[\mathcal{S},\tilde{\mathcal{O}}]+\ldots, \tag{4}$$

where $\tilde{\mathcal{O}}\equiv\mathcal{O}(p\to\tilde{p},d\to\tilde{d},\ldots)$ and

$$\mathcal{S}=\frac{1}{\Delta}(\tilde{\mathcal{T}}_{\Delta}-\tilde{\mathcal{T}}^{\dagger}_{\Delta})+\frac{1}{U-\Delta}(\tilde{\mathcal{T}}_{U-\Delta}-\tilde{\mathcal{T}}^{\dagger}_{U-\Delta})+O(t^2) \tag{5}$$

is the generator of the canonical transformation with

$$\tilde{\mathcal{T}}_{\Delta}=-t\sum_{i,\delta,\sigma}\tilde{p}^{\dagger}_{i+\delta,\sigma}\tilde{d}_{i,\sigma}(1-\tilde{n}^d_{i,\bar{\sigma}}),$$

$$\tilde{\mathcal{T}}_{U-\Delta}=-t\sum_{i,\delta,\sigma}\tilde{d}^{\dagger}_{i,\sigma}\tilde{p}_{i+\delta,\sigma}\tilde{n}^d_{i,\bar{\sigma}}. \tag{6}$$

The subscript $nU+m\Delta$ denotes that the state acted upon is promoted to a subspace at this energy difference. In other words

$$[\tilde{\mathcal{U}},\mathcal{O}_{nU+m\Delta}]=(nU+m\Delta)\mathcal{O}_{nU+m\Delta}, \tag{7}$$

and every operator can be decomposed as $\mathcal{O}=\Sigma_{n,m}\mathcal{O}_{nU+m\Delta}$ with n integers and m integers or half-odd integers. Then $\mathcal{H}_{\text{eff}}$ is given by

$$\mathcal{H}_{\text{eff}}=\tilde{\mathcal{U}}+\tilde{\mathcal{V}}+\frac{1}{\Delta}[\tilde{\mathcal{T}}_{\Delta},\tilde{\mathcal{T}}^{\dagger}_{\Delta}]+\frac{1}{U-\Delta}[\tilde{\mathcal{T}}_{U-\Delta},\tilde{\mathcal{T}}^{\dagger}_{U-\Delta}]+O(t^2). \tag{8}$$

Separating the different processes, $\mathcal{H}_{\text{eff}}=\mathcal{U}'+\mathcal{H}_0+\mathcal{H}_1+\mathcal{H}_2$, and introducing the effective hopping amplitudes $t_S=t^2/(U-\Delta)$ and $t_T=t^2/\Delta$, furthermore, $U'=U+4t_T+4t_S$ and $\Delta'=\Delta+4t_T$, we get (see also Refs. 24 and 25):

$$\mathcal{U}'=\frac{\Delta'}{2}\sum_i(\tilde{n}^p_{i+1/2}-\tilde{n}^d_i)+U'\sum_i\tilde{n}^d_{i,\uparrow}\tilde{n}^d_{i,\downarrow}+V\sum_{i,\delta}\tilde{n}^d_i\tilde{n}^p_{i+\delta},$$

$$\mathcal{H}_0=-t_T\sum_{i,\sigma,\delta}(1-\tilde{n}^d_{i+2\delta,\bar{\sigma}})\tilde{d}^{\dagger}_{i+2\delta,\sigma}\tilde{d}_{i,\sigma}(1-\tilde{n}^d_{i,\bar{\sigma}}),$$

$$\mathcal{H}_1=(t_S+t_T)\sum_{i,\delta,\delta',\sigma}(\tilde{p}^{\dagger}_{i+\delta,\sigma}\tilde{d}^{\dagger}_{i,\bar{\sigma}}\tilde{d}_{i,\sigma}\tilde{p}_{i+\delta',\bar{\sigma}}-\tilde{p}^{\dagger}_{i+\delta,\sigma}\tilde{n}^d_{i,\bar{\sigma}}\tilde{p}_{i+\delta',\sigma})+t_T\sum_{i,\sigma,\delta}\tilde{p}^{\dagger}_{i+\delta,\sigma}\tilde{p}_{i-\delta,\sigma},$$

$$\mathcal{H}_2=t_S\sum_{i,\sigma,\delta}\tilde{n}^d_{i+2\delta,\bar{\sigma}}\tilde{d}^{\dagger}_{i+2\delta,\sigma}\tilde{d}_{i,\sigma}\tilde{n}^d_{i,\bar{\sigma}}. \tag{9}$$

$\mathcal{H}_0$ and $\mathcal{H}_2$ describe the motion of the empty and doubly occupied site, respectively, while $\mathcal{H}_1$ is responsible for the dynamics of the hole on oxygen. By using the Heisenberg model ground state $|\text{GS}\rangle$ for the insulating case, the main effect of the (fourth order) antiferromagnetic (AF) interaction[26] between Cu spins is accounted for.

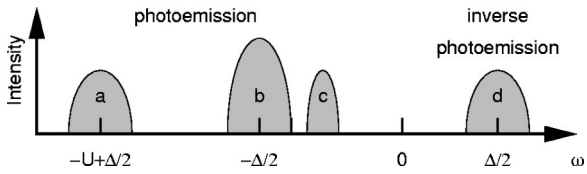

FIG. 2. Schematic distribution of the weights in the strong-coupling limit for a charge-transfer insulator.

III. SPECTRAL FUNCTIONS

Now let us turn to the spectral functions. The photoemission spectrum is proportional to the single particle spectral function, defined by

$$B(k,\omega)=\sum_{f,\sigma}|\langle f|p^{\dagger}_{k,\sigma}|\mathrm{GS}\rangle|^2\delta(\omega+E_f-E_{\mathrm{GS}})+\sum_{f,\sigma}|\langle f|d^{\dagger}_{k,\sigma}|\mathrm{GS}\rangle|^2\delta(\omega+E_f-E_{\mathrm{GS}}),\quad(10)$$

assuming that the cross sections of the Cu and O electron removal are equal. The sum is over final states $|f\rangle$ with a hole added, and a similar definition holds for the inverse photoemission spectra, where a hole is removed. First, we will present the analytical and numerical calculation of the spectral function for the effective model, and then we will compare our results to the spectral function of t-J model and the photoemission spectra of $SrCuO_2$ and Sr_2CuO_3.

A. Calculation of spectral functions

Since the nearest-neighbor Coulomb repulsion leads only to a uniform shift of the final-state energies in the spectral functions, it will be neglected in this section. The strong-coupling behavior of the photoemission spectra is schematically shown in Fig. 2: the hole can go either to the Cu site (peak ''a'') or to the O site (peaks ''b'' and ''c''). The creation operator $c^{\dagger}_{k,\sigma}=d^{\dagger}_{k,\sigma},p^{\dagger}_{k,\sigma}$ entering the calculation of the spectral function Eq. (10) can be decomposed in leading order as $c^{\dagger}_{k,\sigma}=c^{\dagger}_{k,\sigma;-\Delta/2}+c^{\dagger}_{k,\sigma;\Delta/2}+c^{\dagger}_{k,\sigma;U-\Delta/2}$ which represent a hybridized mixture of Cu and O atomic states. For example, including $O(t)$ corrections

$$p^{\dagger}_{i+\delta,\sigma;\Delta/2}=\tilde{p}^{\dagger}_{i+\delta,\sigma}+O(t^2),\quad(11)$$

$$d^{\dagger}_{i,\sigma;\Delta/2}=-\frac{t}{\Delta}\sum_{\delta}\left[(1-\tilde{n}^{d}_{i,\bar{\sigma}})\tilde{p}^{\dagger}_{i+\delta,\sigma}-\tilde{d}^{\dagger}_{i,\sigma}\tilde{p}^{\dagger}_{i+\delta,\bar{\sigma}}\tilde{d}_{i,\bar{\sigma}}\right]+\frac{t}{U-\Delta}\sum_{\delta}\left[\tilde{n}^{d}_{i,\bar{\sigma}}\tilde{p}^{\dagger}_{i+\delta,\sigma}+\tilde{d}^{\dagger}_{i,\sigma}\tilde{p}^{\dagger}_{i+\delta,\bar{\sigma}}\tilde{d}_{i,\bar{\sigma}}\right]+O(t^2).\quad(12)$$

The final states in peaks b and c are obtained by applying $c^{\dagger}_{k,\sigma;\Delta/2}$ to the ground state, and the sum rule of the b + c peaks in Fig. 2 is

$$\langle \mathrm{GS}|p_{k,\sigma;\Delta/2}p^{\dagger}_{k,\sigma;\Delta/2}|\mathrm{GS}\rangle+\langle \mathrm{GS}|d_{k,\sigma;\Delta/2}d^{\dagger}_{k,\sigma;\Delta/2}|\mathrm{GS}\rangle=1+O(t^2).\quad(13)$$

Similarly, the weight in peaks a and d is $1/2+O(t^2)$. For simplicity, we do not include the corrections in Eq. (12) when we calculate the spectral functions.

The dynamics in the peak a is governed by $\mathcal{H}_2$: the extra hole on Cu, created by $\tilde{d}^{\dagger}_{k,\sigma}$ in Eq. (10), hops to neighboring Cu sites with amplitude t_S, leaving the spin sequence unchanged:

$$\mathcal{H}_2|\cdots\sigma_{j-1}2\sigma_j\cdots\rangle=-t_S|\cdots 2\sigma_{j-1}\sigma_j\cdots\rangle-t_S|\cdots\sigma_{j-1}\sigma_j 2\cdots\rangle.\quad(14)$$

Here ''2'' in the wave function denotes the position of the extra hole (site occupied by two holes), and σ_j the spins of the singly occupied Cu sites with $j=1,\ldots,L-1$, as there are $L-1$ spins remaining. The situation is identical to the case of $U/t\to+\infty$ Hubbard model, where we know that the wave function of a state with momentum k factorizes into charge and spin parts:[2–4]

$$|f_Q(k)\rangle=\frac{1}{\sqrt{L}}\sum_{j=0}^{L-1}e^{i(k-Q)j}|\psi_j\rangle\otimes|\chi_{L-1}(Q,n_Q)\rangle,\quad(15)$$

where $|\psi_j\rangle$ describes free spinless fermions on L lattice points with an empty site j, which in our case is the site with the extra hole. $|\chi_{L-1}(Q,n_Q)\rangle$ is the squeezed spin-wave function of $L-1$ spins with momentum $Q=2\pi J/(L-1)$, J integer, and other quantum numbers n_Q. The energy of the state is

$$\varepsilon_Q(k)=U'-\Delta'/2-2t_S\cos(k-Q).\quad(16)$$

Now that we have both the energy and the wave function of the final state, we are ready to calculate the spectral function as presented by Sorella and Parola for the large-U Hubbard model.[3] As a first step, we write the ground state also in a product form

$$|\mathrm{GS}\rangle=|\psi_{\mathrm{GS}}\rangle\otimes|\chi_{\mathrm{GS}}\rangle,\quad(17)$$

where the $|\chi_{\mathrm{GS}}\rangle$ is the Heisenberg ground-state wave function and $|\psi_{\mathrm{GS}}\rangle$ is the fully filled Fermi see of spinless fermions (charges). It is convenient to choose systems with 2, 6, 10, etc. sites, where the momentum of the $|\mathrm{GS}\rangle$ is zero. In the matrix element of Eq. (10) it suffices to keep the momentum dependence in the final wave function only,

$$|\langle f_Q(k)|\tilde{d}^{\dagger}_{k,\sigma}|\mathrm{GS}\rangle|^2=L|\langle f_Q(k)|\tilde{d}^{\dagger}_{j=0,\sigma}|\mathrm{GS}\rangle|^2=|\langle\chi(Q,n_Q)|Z_{0,\sigma}|\chi_{\mathrm{GS}}\rangle|^2,\quad(18)$$

where we have substituted the factorized form Eq. (15) and used the fact that the overlap in the charge part is 1. Only the spin part is nontrivial: the operator $Z_{j,\sigma}$ removes a spin σ at site j, reducing the spin sequence to length $L-1$. Introducing

$$D(Q)=\sum_{n_Q}|\langle\chi(Q,n_Q)|Z_{0,\sigma}|\chi_{\mathrm{GS}}\rangle|^2\quad(19)$$

for the spectral function we get

$$B(k,\omega)=\sum_{Q}D(Q)\,\delta[\omega+\varepsilon_Q(k)].\quad(20)$$

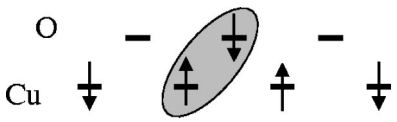

FIG. 3. The state $|\downarrow\vec{S}\uparrow\downarrow\rangle$. The Cu and O spins in the shaded region form a singlet, which we denoted by $\vec{S}$.

$D(Q)$ is essentially the ''occupation number'' of the spinons, and has a singularity at the spinon Fermi momenta $Q=\pm\pi/2$. It can be approximated as $(L-1)D(Q)\approx -0.5+2.98/\sqrt{\pi^2-4Q^2}$ for $-\pi/2<Q<\pi/2$ and zero otherwise.[3,4,27] We therefore find that the spectral function in the upper Hubbard band (peak a) is identical to that of the large-U Hubbard or small J t-J model. Note also that the inverse photoemission spectrum will have a similar form with bandwidth $4t_T$ (peak d in Fig. 2).

Let us now proceed to peaks b and c in Fig. 2, which can be associated with the hole on oxygens. The hole added to an O site with $\tilde{p}^\dagger_{k,\sigma}$ can form a singlet or triplet with a neighboring Cu spin. We will denote by $|\tilde{S}\rangle$ ($|\vec{S}\rangle$) states where the O hole forms a singlet with the Cu spin on its right (left), as seen in Fig. 3. For example,

$$|\downarrow\vec{S}\uparrow\downarrow\rangle=\frac{1}{\sqrt{2}}\tilde{d}^\dagger_{1\downarrow}(\tilde{d}^\dagger_{2\uparrow}\tilde{p}^\dagger_{5/2\downarrow}-\tilde{d}^\dagger_{2\downarrow}\tilde{p}^\dagger_{5/2\uparrow})\tilde{d}^\dagger_{3\uparrow}\tilde{d}^\dagger_{4\downarrow}|0\rangle,$$

$$|\downarrow\tilde{S}\uparrow\downarrow\rangle=\frac{1}{\sqrt{2}}\tilde{d}^\dagger_{1\downarrow}(\tilde{p}^\dagger_{3/2\downarrow}\tilde{d}^\dagger_{2\uparrow}-\tilde{p}^\dagger_{3/2\uparrow}\tilde{d}^\dagger_{2\downarrow})\tilde{d}^\dagger_{3\uparrow}\tilde{d}^\dagger_{4\downarrow}|0\rangle.$$

As we will see below, a suitable combination of these states will give us the Zhang-Rice singlets,[12] in terms of which the lowest energy excitations may be described by a one band model. In the present calculation we are also including the triplets and high-energy singlets in order to describe higher energy excitations. Note that this basis is not orthogonal:

$$\langle\cdots\vec{S}\sigma\cdots|\cdots\vec{S}\sigma\cdots\rangle=1,$$

$$\langle\cdots\vec{S}\sigma\cdots|\cdots\sigma\tilde{S}\cdots\rangle=1/2. \tag{21}$$

In general, the resulting spectrum is complicated and the singlets and triplets mix with one other, except for the particular case of t_S finite and $t_T=0$.[25,28] Due to the very special form of $\mathcal{H}_1$ for $t_T=0$

$$\mathcal{H}_1=-2t_S\sum_{i,\delta,\delta',\alpha,\alpha'}\left(\frac{\delta_{\alpha\alpha'}}{4}\tilde{n}^d_i-\frac{\boldsymbol{\tau}_{\alpha\alpha'}}{2}\tilde{\mathbf{S}}^d_i\right)\tilde{p}^\dagger_{i+\delta,\alpha}\tilde{p}_{i+\delta',\alpha'}, \tag{22}$$

where we can identify the projector onto spin singlets (here $\tilde{\mathbf{S}}^d_i=\Sigma_{\sigma,\sigma'}\tilde{d}^\dagger_{i,\sigma}\boldsymbol{\tau}_{\sigma\sigma'}\tilde{d}_{i,\sigma'}/2$ and $\boldsymbol{\tau}$ is the vector of Pauli matrices), the matrix elements of $\mathcal{H}_{\rm eff}$ leading to propagation of the singlets are

$$\mathcal{H}_1|\cdots\vec{S}\sigma\cdots\rangle=t_S|\cdots\sigma(\vec{S}-\tilde{S})\cdots\rangle-2t_S|\cdots(\vec{S}-\tilde{S})\sigma\cdots\rangle,$$

$$\mathcal{H}_1|\cdots\sigma\tilde{S}\cdots\rangle=-t_S|\cdots(\vec{S}-\tilde{S})\sigma\cdots\rangle+2t_S|\cdots\sigma(\vec{S}-\tilde{S})\cdots\rangle.$$

The combination $|\vec{S}\rangle-|\tilde{S}\rangle$ moves through the lattice like the site ''2'' in Eq. (14)

$$\begin{aligned}\mathcal{H}_1|\cdots\sigma_{j-1}(\vec{S}-\tilde{S})\sigma_j\cdots\rangle&=t_S(|\cdots\sigma_{j-1}\sigma_j(\vec{S}-\tilde{S})\cdots\rangle\\&\quad-4|\cdots\sigma_{j-1}(\vec{S}-\tilde{S})\sigma_j\cdots\rangle\\&\quad+|\cdots(\vec{S}-\tilde{S})\sigma_{j-1}\sigma_j\cdots\rangle),\end{aligned} \tag{23}$$

leaving the spin sequence unchanged. In this case $|\psi_j\rangle$ in Eq. (15) will denote this particular combination at site j. The energy of the state is

$$\varepsilon^S_Q(k)=\Delta/2-4t_S+2t_S\cos(k-Q). \tag{24}$$

These singlets leads to the formation of the c peak in Fig. 2.

Next, we need to calculate the matrix elements. Using the identity

$$|\langle f|\tilde{p}^\dagger_{k,\sigma}|\mathrm{GS}\rangle|^2=L|\langle\mathrm{GS}|\tilde{p}_{1/2,\sigma}|f(k)\rangle|^2, \tag{25}$$

where $p_{1/2,\sigma}$ removes the hole at site $i=1/2$, the k dependence is now in the final state only. So, for the matrix element we get

$$\begin{aligned}&L|\langle\mathrm{GS}|\tilde{p}_{1/2,\downarrow}|f(k)\rangle|^2\\&=|\sum_j e^{i(k-Q)j}(\langle\chi_{\rm GS}|\otimes\langle\psi_{\rm GS}|)\tilde{p}_{1/2,\downarrow}\\&\quad\times(|\psi_j\rangle\otimes|\chi(Q,n_Q)\rangle)|^2\\&=\frac{1}{2}|\langle\chi_{\rm GS}|(Z^\dagger_{0,\uparrow}-e^{i(k-Q)}Z^\dagger_{1,\uparrow})|\chi(Q,n_Q)\rangle|^2\\&=(1+\cos k)|\langle\chi_{\rm GS}|Z^\dagger_{0,\uparrow}|\chi(Q,n_Q)\rangle|^2,\end{aligned} \tag{26}$$

where we have used that $\langle\chi_{\rm GS}|Z^\dagger_{1,\uparrow}|\chi(Q)\rangle=-e^{iQ}\langle\chi_{\rm GS}|Z^\dagger_{0,\uparrow}|\chi(Q)\rangle$. Dividing the matrix element by the norm of the final state

$$\langle f_Q(k)|f_Q(k)\rangle=2-\cos(k-Q)=\frac{\Delta-2\varepsilon^S_Q(k)}{4t_S}, \tag{27}$$

and summing over final states with definite Q, we can write the spectral function as

$$B_S(k,\omega)=\frac{4t_S(1+\cos k)}{\Delta+2\omega}\sum_Q D(Q)\,\delta[\omega+\varepsilon^S_Q(k)]. \tag{28}$$

Clearly, even introducing form factors in the one band model [which is identical in form to Eq. (20)], the ω-dependent prefactor of the spectral distribution above cannot be obtained. The local (k-averaged) spectral function for the singlets is

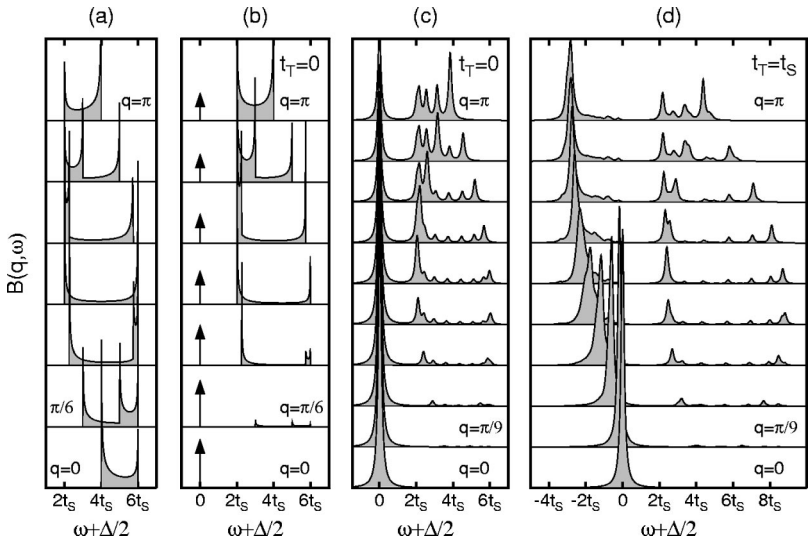

FIG. 4. The analytical result for photoemission spectra of (a) t-J model in the $J/t\rightarrow 0$ limit [Eq. (28) without the k and ω dependent prefactors] and (b) $t_T=0$ effective model [Eq. (28)], compared to (c) a Lánczos diagonalization of 18 site effective model for $t_T=0$ and (d) $t_T=t_S$. The δ functions are plotted as Lorentzians of width 0.1. The $q=k+\pi$ is the momentum when the relative phases of d and p orbitals are properly included and it should be used when we compare with the experiments.

$$B_S(\omega)=\frac{1}{\pi}\frac{4t_S+(2\ln 2-1)(-2\omega-\Delta+8t_S)}{(\Delta+2\omega)\sqrt{(\Delta-4t_S+2\omega)(-2\omega-\Delta+12t_S)}}, \tag{29}$$

with weight 0.32. The rest of the weight (0.68) is at higher energies $\omega=-\Delta/2$, where we find nondispersing solutions, made of a particular combination of singlets $|\vec{S}\sigma\sigma'\rangle-2|\sigma\vec{S}\sigma'\rangle-2|\sigma\bar{S}\sigma'\rangle+|\sigma\sigma'\bar{S}\rangle$, as well as the triplets, contributing with a delta peak to the spectral function to form the peak b in Fig. 2.

The only requirement for the procedure outlined above to work is that during the motion of the hole the spin sequence is unchanged. This immediately requires $t_T=0$ in $\mathcal{H}_1$.

The influence of finite t_T is shown in Fig. 4. The lower ''singlet'' band increases its width, while the overall shape of $B_S(k,\omega)$ does not change significantly. On the other hand, peak b now extends from $\Delta/2$ to $\Delta/2+4t_T$ and a sharp dispersion dominates the spectrum. Only a slight weight transfer from the ''singlet'' to the ''triplet'' band can be observed, e.g., at $k=0$ $(q=\pi)$ the weight in the singlet band is reduced from 0.65 to 0.43 as we increase t_T from 0 to t_S, while the total weight, given by Eq. (13) is unchanged in leading order.

B. Comparison with the t-J model and photoemission experiments

Comparing with the t-J model for small J [Fig. 4(a)], we can see that although (also for $t_T=t_S$) the singlet feature is similar to the t-J model result,[3] there are detailed differences in the distribution of weight, similar to those in Eq. (28), as well as in the dispersion of the upper edge of the singlet continuum. We therefore see that even in parameter regimes where the one band t-J description accurately predicts low-energy excitation energies, the two band model may have significantly different properties as far as other physical observables is concerned, exemplified here by the momentum and frequency dependence of the spectral weights. The effect of finite J is to give dispersion to the now dispersionless lower ''spinon'' edge in both Emery and t-J model.

Finally, let us compare our results with the experiments. For both $SrCuO_2$ and Sr_2CuO_3 the low-energy region shows features found in the t-J model, i.e., the holon and spinon bands dispersing with $t\approx 0.5$–0.6 eV and $J\approx 0.15$–0.2 eV, respectively, which is consistent with the susceptibility,[5] optical,[29] and electron-energy-loss[11] experiments. However, an additional interesting feature is the weight reduction as the zone center $(q=0)$ is approached. In Refs. 7 and 10 this is attributed to the different cross sections of Cu and O orbitals, while in our theory it arises quite naturally from the internal structure of the low-energy singlets. Concerning the higher energy features, the triplet feature is in reasonable agreement with the dispersing peak at 2 eV in Fig. 6 of Ref. 8, if one disregards the flat nonbonding oxygen bands not included in our model. These general trends do not depend strongly on t_T/t_S and the inclusion of t/Δ and $t/(U-\Delta)$ correction in operators leads only to a small weight transfer to lower energies.

IV. DENSITY-DENSITY CORRELATIONS

The density-density correlation function describes the dynamical dielectric response of the material and is accessible by measuring, e.g., the optical conductivity, electron-energy-loss spectra (EELS), and inelastic x-ray scattering. Both optical conductivity[30] and EELS (Ref. 11) have been measured on Sr_2CuO_3. The EELS spectra can be reasonably well interpreted within a one band Hubbard model extended with nearest-neighbor repulsion, so it is interesting to see what changes if we consider a two band model, like the Emery model.

Since the system is an insulator, we get finite density response only above the charge transfer gap at $\omega\approx\Delta$. In lowest order the density-density correlation function is given by

$$\mathcal{N}(k,\omega)=\sum_f |\langle f|n_{k;\Delta}|\mathrm{GS}\rangle|^2\delta(\omega-E_f+E_{\mathrm{GS}}), \tag{30}$$

where $n_{k;\Delta}=n^d_{k;\Delta}+n^p_{k;\Delta}$ can be calculated from $n_{i;\Delta}=(1/\Delta)[\tilde{\mathcal{T}}_\Delta,\tilde{n}_i]$ and reads

$$n_{k;\Delta}=\frac{t}{\Delta}\frac{1}{\sqrt{L}}\sum_{j,\delta,\sigma} e^{ikj}(e^{i\delta k}-1)(1-\tilde{n}_{j,\bar{\sigma}})\tilde{p}^\dagger_{j+\delta,\sigma}\tilde{d}_{j,\sigma}. \tag{31}$$

This leads to the sum rule

$$\int \mathcal{N}(k,\omega)d\omega = 8\frac{t^2}{\Delta^2}\sin^2\frac{k}{4}. \tag{32}$$

Now let us determine the dynamical density response in the special case $t_T=0$. The operator $n_{k;\Delta}$ moves a hole from Cu to O, and results in a two-body problem, which can be solved using standard techniques. For the singlet part, the final-state wave function can be represented as

$$|f_S\rangle = \sum_{j=1}^{L-1} (x_j|e\sigma_1\cdots\sigma_{j-1}\tilde{S}\sigma_j\cdots\rangle$$

$$-y_j|e\sigma_1\cdots\sigma_{j-1}\vec{S}\sigma_j\cdots\rangle), \tag{33}$$

with the norm

$$\langle f_S|f_S\rangle = \sum_{j=1}^{L-1}(x_j^2+y_j^2) - \sum_{j=1}^{L-2} y_j x_{j+1}. \tag{34}$$

These states are L-fold degenerate, since ''e,'' which represents the Cu with no hole, does not hop in this limit. The Schrödinger equation gives

$$Ex_j = Ey_j = t_S(x_{j+1}-2x_j-2y_j+y_{j-1}) \tag{35}$$

for $j=2,\ldots,L-2$ with boundary conditions

$$Ey_1 = t_S(x_2-2x_1-2y_1),$$

$$E(y_1-x_1) = Vx_1,$$

$$Ey_{L-1} = t_S(x_{L-2}-2x_{L-1}-2y_{L-1}),$$

$$E(y_{L-1}-x_{L-1}) = Vx_{L-1}.$$

The energy E is measured from Δ. Due to symmetry x_j and y_j are real and there are even and odd parity solutions with $x_j = \mp y_{L-j}$.

Let us first consider the case $V=0$. We immediately see that $(x_j-y_j)E=0$, i.e., $x_j=y_j$ for $E\neq 0$ and $j=1,\cdots,(L-1)$. The solution is $x_j=y_j=\sin j\kappa$, with $\kappa = I\pi/L$, and $I=1,2,\cdots,L-1$. These states have even (odd) parity for I even (odd), energy

$$E_\kappa = -4t_S+2t_S\cos\kappa, \tag{36}$$

and norm $\langle f_S|f_S\rangle = L(2-\cos\kappa)/2$. For $L\to\infty$ they will form a continuum from $E=-6t_S$ to $-2t_S$. Additionally there are $L-1$ degenerate states with $E=0$. The matrix elements in Eq. (30) for the singlet contribution read

$$|\langle f_S|n_{k;\Delta}|\mathrm{GS}\rangle|^2 = \frac{8t^2}{\Delta^2}F_S\frac{x_1^2}{\langle f|f\rangle}\left[1\pm\cos\frac{k}{2}\right]\sin^2\frac{k}{4}, \tag{37}$$

where the $+$ $(-)$ sign is for the even (odd) state, and $F_S = \langle \mathrm{GS}|\frac{1}{4}-\mathbf{S}_0\cdot\mathbf{S}_1|\mathrm{GS}\rangle \to \ln 2$ for $L\to\infty$ is the probability of finding two neighboring spins forming a singlet in the spin sequence. The only nontrivial quantity is $x_1^2/\langle f_S|f_S\rangle$, which can be conveniently expressed using the energy of the state as

$$\frac{x_1^2}{\langle f|f\rangle} = \frac{1}{L}\frac{2\sin^2\kappa}{2-\cos\kappa} = \frac{1}{L}\frac{(2t_S+E)(6t_S+E)}{t_S E}. \tag{38}$$

In the thermodynamic limit we replace the sum over states with an integral over energy:

$$\sum_I \to \int dE_\kappa \frac{1}{\pi}\frac{\partial\kappa}{\partial E_\kappa}, \tag{39}$$

where $(1/\pi)(\partial\kappa/\partial E_\kappa)$ is the density of states

$$\frac{1}{\pi}\frac{\partial\kappa}{\partial E_\kappa} = \frac{1}{\pi}\frac{1}{\sqrt{(-2t_S-E)(6t_S+E)}}, \tag{40}$$

the factor $[1\pm\cos(k/2)]$ in Eq. (37) averages to 1, and for the contribution of the Zhang-Rice singlets to the density response we get

$$\mathcal{N}(k,\omega) = \frac{8\ln 2}{\pi}\frac{t^2}{\Delta^2}\frac{\sqrt{(\omega-\Delta+6t_S)(\Delta-2t_S-\omega)}}{t_S(\Delta-\omega)}\sin^2\frac{k}{4}. \tag{41}$$

The density response in this limit has a trivial momentum dependence, due to the nondispersing nature of the ''e'' site. It gives $2(2-\sqrt{3})F_S \approx 37\%$ of the total weight, the rest of the weight is in a single peak at $\omega=\Delta$, which comes from the nondispersing singlets and triplets. The $\mathcal{N}(k,\omega)$ we just calculated is shown on the upper left plot in Fig. 5.

Turning on the Cu-O repulsion, which acts as an effective attraction between the empty Cu site and the O hole, two twofold degenerate (for $L\to\infty$) excitons with energies

$$\Omega_S^{\pm} = \frac{3t_S V+V^2 \pm V\sqrt{12t_S^2+V^2}}{t_S-2V} \tag{42}$$

appear, together with a twofold degenerate exciton involving the triplets at $\Omega_T=-V$. The Ω_S^+ solution exists only for $V>2t_S$ where it splits off from the lower edge of the continuum. Not going into the details, the expression for $x_1^2/\langle f_S|f_S\rangle$ in Eq. (37) now reads

$$\frac{x_1^2}{\langle f|f\rangle} = \frac{-E(2t_S+E)(6t_S+E)}{24t_S^2V+2E(4t_S-V)V+L[(2V-t_S)E^2+2(3t_S+V)VE+3V^2t_S]}, \tag{43}$$

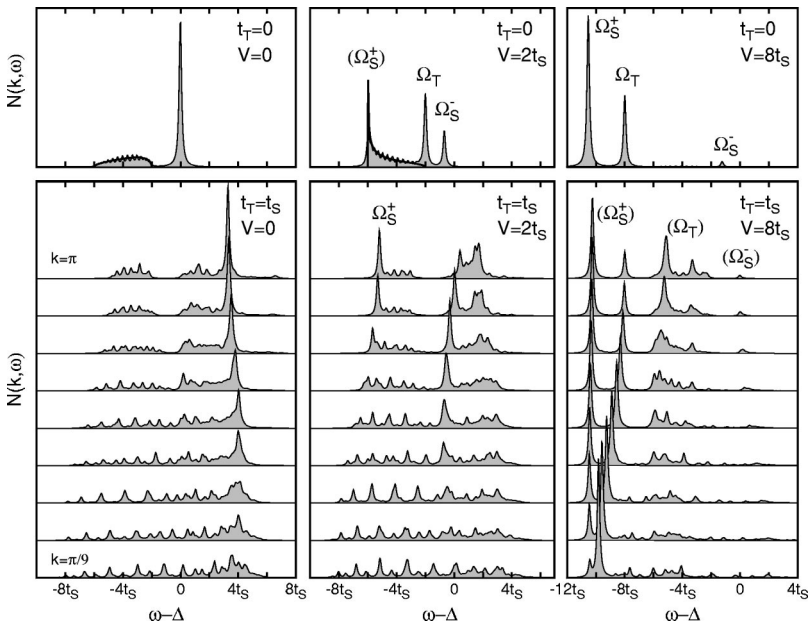

FIG. 5. $\mathcal{N}(k,\omega)$ of 18 site effective model for $V=0$, $2t_S$, and $8t_S$ from left to the right, and $t_T=0$ (upper) and $t_T=t_S$ (lower plots) obtained by exact diagonalization. The thick line in the upper plots shows the analytical result. The δ functions are plotted as Lorentzians of width $0.1t_S$ and the plots for each k are normalized to have total weight 1. In the upper plots we show $k=\pi$ only because of the trivial k dependence. The remnants of excitons are indicated within the parenthesis in the lower right plot. These spectra are independent of the phase factors of Cu and O orbitals.

which is valid both for the $\Omega_S^{\pm}$ excitons and the continuum. The $\mathcal{N}(k,\omega)$ is complicated and we do not give the analytical form, which is straightforward to derive from Eqs. (37), (40), and (43), but we refer to Fig. 5 for a discussion of features. For small V the energy of the exciton is $\Omega_S^- \approx (3-2\sqrt{3})V$ with relative weight $\approx [2\sqrt{3}-3-2(7-4\sqrt{3})V/t_S]F_S$, i.e., increasing V the weight is transferred to the continuum. For large repulsion ($t_S \ll V \ll U$) the weight is concentrated in the excitons at $\Omega_S^+ \approx -V-2t_S$, while the continuum and the exciton at $\Omega_S^- \approx -3t_S/2$ has a negligible weight of the order of t_S^2/V^2. On the other hand, the triplet exciton Ω_T has weight $1-F_S \approx 31\%$, independent of the size of V.

To study the effect of finite t_T, we used numerical Lánczos diagonalization of small systems (18 site) to extract the density-density correlations. As can be seen in Fig. 5, the effect of finite t_T is substantial: (i) Because ''*e*'' acquires dispersion, the shape of the spectrum resembles more closely that of the one band model, in that it narrows as $k \to \pi$.[31] Turning on V, excitonic features are formed at the zone boundary. (ii) The contributions coming from singlets and triplets cannot be separated energetically, especially for small momenta. (iii) While for $t_T=0$ the excitons are sharp peaks, for $t_T \neq 0$ these sharp excitonic peaks broaden and form an incoherent spectrum. A direct comparison with the experiments to decide whether a two band model is more appropriate is difficult, given that the resolution of the EELS spectra is not sufficient to see the detailed differences between the two band and the one band models. Furthermore, all of our results here are valid in the strong-coupling limit, so one expects quantitative changes to the spectra for experimentally relevant coupling strengths.

Recently, the density response was calculated using projection techniques in Ref. 32, with a result which disagrees with ours. Since the calculation presented in that paper is rather involved, it is difficult to trace whether the difference is due to the method applied or to the parameter regime investigated.

V. CONCLUSION

We have demonstrated that spin-charge factorization may be applied to understand dynamical behavior of the two band model in a particular limit. The low-energy hole charge carriers have been identified as complex objects resembling Zhang-Rice singlets, and the low-energy part of the single-particle spectral function of the two-band model has been shown to be related to that of the one band model with nontrivial frequency as well as momentum dependent corrections. This provides a very simple and natural explanation for the momentum and frequency dependence of the spectral weights observed experimentally.

ACKNOWLEDGMENTS

We would like to thank Professor P. Fulde for his kind hospitality in Max-Planck-Institute für Physik komplexer Systeme in Dresden, where the present work started. This work was partially funded by Hungarian OTKA D32689, AKP98-66, and Bolyai 118/99.

[1] J. Sólyom, Adv. Phys. **28**, 201 (1979).

[2] F. Woynarovich, J. Phys. C **15**, 97 (1982); M. Ogata and H. Shiba, Phys. Rev. B **41**, 2326 (1990).

[3] S. Sorella and A. Parola, J. Phys.: Condens. Matter **4**, 3589 (1992).

[4] K. Penc, K. Hallberg, F. Mila, and H. Shiba, Phys. Rev. B **55**, 15 475 (1997).

[5] N. Motoyama, H. Eisaki, and S. Uchida, Phys. Rev. Lett. **76**, 3212 (1996), and references therein.

[6] C. Kim, A. Y. Matsuura, Z.-X. Shen, N. Motoyama, H. Eisaki, S. Uchida, T. Tohyama, and S. Maekawa, Phys. Rev. Lett. **77**, 4054 (1996).

[7] C. Kim, Z.-X. Shen, N. Motoyama, H. Eisaki, S. Uchida, T. Tohyama, and S. Maekawa, Phys. Rev. B **56**, 15 589 (1997).

[8] N. Nagasako, T. Oguchi, H. Fujisawa, O. Akaki, T. Yokoya, T. Takahashi, M. Tanaka, M. Hasegawa, and H. Takei, J. Phys. Soc. Jpn. **66**, 1756 (1997).
[9] H. Fujisawa, T. Yokoya, T. Takahashi, S. Miyasaka, M. Kibune, and H. Takagi, Solid State Commun. **106**, 543 (1998).
[10] H. Fujisawa, T. Yokoya, T. Takahashi, S. Miyasaka, M. Kibune, and H. Takagi, Phys. Rev. B **59**, 7358 (1999).
[11] R. Neudert, M. Knupfer, M. S. Golden, J. Fink, W. Stephan, K. Penc, N. Motoyama, H. Eisaki, and S. Uchida, Phys. Rev. Lett. **81**, 657 (1998).
[12] F. C. Zhang and T. M. Rice, Phys. Rev. B **37**, 3759 (1988).
[13] S. Sorella and A. Parola, Phys. Rev. Lett. **76**, 4604 (1996); Phys. Rev. B **57**, 6444 (1998); J. Voit, Eur. Phys. J. B **5**, 505 (1998).
[14] Y. Kato, Phys. Rev. Lett. **81**, 5402 (1998); H. Suzuura and N. Nagaosa, Phys. Rev. B **56**, 3548 (1997).
[15] R. Eder and Y. Ohta, Phys. Rev. B **56**, 2542 (1997).
[16] F. Gebhard, K. Bott, M. Scheidler, P. Thomas, and S. W. Koch, Philos. Mag. B **75**, 47 (1997); T. Fujii and N. Kawakami, J. Phys. Soc. Jpn. **68**, 2331 (1999); E. Jeckelmann, F. Gebhard, and F. H. L. Essler, cond-mat/9911281 (unpublished); D. Controzzi, F. H. L. Essler, and A. M. Tsvelik, cond-mat/0005349 (unpublished); J. M. P. Carmelo, M. N. Peres, and P. D. Sacramento, Phys. Rev. Lett. **84**, 4673 (2000).
[17] V. J. Emery, Phys. Rev. Lett. **58**, 2794 (1987).
[18] C. Vermeulen, W. Barford, and E. R. Gagliano, Europhys. Lett. **31**, 225 (1995); A. Sudbø, S. Schmitt-Rink, and C. M. Varma, Phys. Rev. B **46**, 5548 (1992).
[19] J. Zaanen, G. A. Sawatzky, and J. W. Allen, Phys. Rev. Lett. **55**, 418 (1985).
[20] H. Rosner, H. Eschrig, R. Hayn, S.-L. Drechsler, and J. Málek, Phys. Rev. B **56**, 3402 (1997).
[21] R. Neudert, S.-L. Drechsler, J. Málek, H. Rosner, M. Kielwein, Z. Hu, M. Knupfer, M. S. Golden, J. Fink, N. Nücker, M. Merz, S. Schuppler, N. Motoyama, H. Eisaki, S. Uchida, M. Domke, and G. Kaindl, Phys. Rev. B **62**, 10 752 (2000).
[22] A. B. Harris and R. V. Lange, Phys. Rev. **157**, 295 (1967).
[23] H. Eskes and A. M. Oleś, Phys. Rev. Lett. **73**, 1279 (1994); H. Eskes, A. M. Oleś, M. B. J. Meinders, and W. Stephan, Phys. Rev. B **50**, 17 980 (1994).
[24] J. Zaanen and A. M. Oleś, Phys. Rev. B **37**, 9423 (1988); P. Prelovšek, Phys. Lett. A **126**, 287 (1988).
[25] V. J. Emery and G. Reiter, Phys. Rev. B **38**, 11 938 (1988).
[26] J. E. Hirsch, Phys. Rev. Lett. **59**, 228 (1987).
[27] J. C. Talstra and S. P. Strong, Phys. Rev. B **56**, 6094 (1997).
[28] F. C. Zhang, Phys. Rev. B **39**, 7375 (1989).
[29] H. Suzuura, H. Yasuhara, A. Furusaki, N. Nagaosa, and Y. Tokura, Phys. Rev. Lett. **76**, 2579 (1996).
[30] K. Maiti, D. D. Sarma, T. Mizokawa, and A. Fujimori, Europhys. Lett. **37**, 359 (1997).
[31] W. Stephan and K. Penc, Phys. Rev. B **54**, R17 269 (1996); K. Tsutsui, T. Tohyama, and S. Maekawa, *ibid.* **61**, 7180 (2000).
[32] J. Richter, C. Waidacher, and K. W. Becker, Phys. Rev. B **61**, 9871 (2000).